A simple design method for surface-mounted PM machines for traction application

(Article begins on next page)

25 April 2024

A Simple Design Method for Surface-mounted PM Machines for Traction Application

Chao Lu and Gianmario Pellegrino

Department of Energy
Politecnico di Torino
Turin, Italy
chao.lu@polito.it, gianmario.pellegrino@polito.it

Abstract— **Surface-mounted permanent magnet motors with concentrated windings (CW-SPM) can have a wide constant power speed range if properly designed. This study introduces a design approach for CW-SPM machines for traction application, presenting the new parametric design plane *x*, *b*, where *x* accounts for the rotor on stator radius split and *b* summarizes the share between copper and iron in the stator. The proposed design method aims at covering the important area of design of PMSMs with flux weakening capability, with a simple methodology. Analytical and finite-element (FEA) models are used jointly. The design flowchart is illustrated and the output designs are validated by FEA. All presented results are obtained through open-source design resources available online.**

Keywords—electrical machine design; concentrated windings; surface mountted permanent magnet; parametric design

I. INTRODUCTION

Permanent magnet synchronous machines (PMSMs) have generated considerable research interest during last decades in view of fast dynamic performance, high torque density and efficiency. In traction applications, PMSMs with concentrated windings have enormous potential, thanks to their low cogging torque and high power density, etc. [1]-[2]. Surface-mounted permanent magnet machines with concentrated windings (CW-SPM) are one the popular solutions for their capability of achieving wide constant power speed range with rather simple geometry an ease of manufacturing [3]. CW-SPM machines can have a high slot fill factor and short end-turns compared to the machines with distributed windings (DW-SPM machines) [4]-[5]. However, the design of CW-SPM machines for traction application is not as well established as the one of DW-SPM machines, and requires the tradeoff between at least two very different operating states, namely the starting torque and power at high speed, in flux weakening conditions.

Targeting multiple working conditions complicates the machine design process and produces some confusion in what the best approach to the design can be. The analysis of CW-SPM machines with high flux weakening capability is illustrated in [6]. The influence of the ratio between the rotor diameter and stator diameter on motor efficiency is reported [7]. Optimization methods have been adopted aiming at minimizing total losses [8]-[9]. For traction applications, the wide torque and speed operating range is a great challenge.

This paper aims at simplifying the design approach by using the nominal power factor (PF) of the machine as the
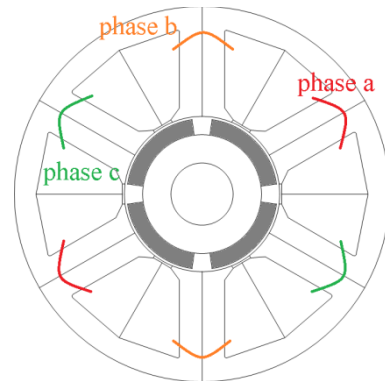

Fig. 1. General structure of a CW-SPM with 6 slots, 2 pole pairs, double layer three phase winding.

metrics for achieving an optimal tradeoff between starting torque and flux weakening capability.

A parametric design approach is introduced, inspired to the general design approach used in [10] for machines with high numbers of poles. Torque and PF at rated current loading are evaluated in the (*x*, *b*) parametric plane, where *x* is the rotor / stator split and *b* is the tooth/slot split. The (*x*, *b*) plane thus represents a continuum of machines with different rotor and stator geometries, all within the same stack envelope.

Among all solutions, the one with PF equal to $1/\sqrt{2}$ and maximum torque is selected, being the one with the highest torque among the ones with infinite flux weakening capability, as shown in the paper. The characteristic current condition is the pivot of this analysis: all advisable designs will have the nominal current equal to their characteristic current [11].

The undertaken design process is implemented with open-source design software available online [12], which integrates sizing equations and magnetic static finite element analysis (FEA), with instruments available online, too [13]. Optimization algorithms and a simple thermal network are also included in the design software, for the sake of design optimization/refinement and for preliminary stator and rotor temperature evaluation, respectively. On this platform, optimization algorithms and FEA can be directly used in the design of the CW-SPM machine. The parametric design method proposed here skips the optimization process and abundant FEA simulations, thereby diminishing design time and suggesting a procedure of general validity.

II. DESIGN PROCEDURE

This paper uses two key design specifications for the design of the electric motor for traction: 1) nominal torque, under the base speed, and 2) nominal power at maximum speed. The key design parameter is the characteristic current of the PMSM, as all investigated designs will respect the condition of having the nominal current equal to the characteristic current:

$$I_{ch} = \frac{\lambda_m}{L_d} = I_n \quad (1)$$

Such design condition turns into an asymptotically flat power versus speed profile in voltage and current limited conditions. For example, see Fig. 2b, continuous line. If (1) holds, the characteristic power (2) is the asymptote of the power vs speed curve, as indicated in Fig. 2b. Reported torque and power profiles refer to the case of a lossless machine.

$$P_{nmax} = P_{ch} = \frac{3}{2} V_{max} I_{ch} \quad (2)$$

The base speed is where flux weakening starts, i.e. when the inverter voltage limit kicks in. Base speed is not an explicit design input in this analysis, as it comes as a consequence of the two key design goals of torque and power, as said. At base speed, output power is:

$$P_{base} = T_n \cdot \omega_{base} = P_{ch}/\sqrt{2} \quad (3)$$

The proposed design flowchart targets power curves of the kinds depicted in Fig. 2: the continuous curve refers to strict respect of (1), whereas the sharper power curve in dashes is obtained imposing $I_n > I_{ch}$ by design (in the example I_{ch} is same as before and I_n is 170% of I_{ch}. In this second case the starting torque is higher, the power profile sharper, and this can be useful, if required by the application.
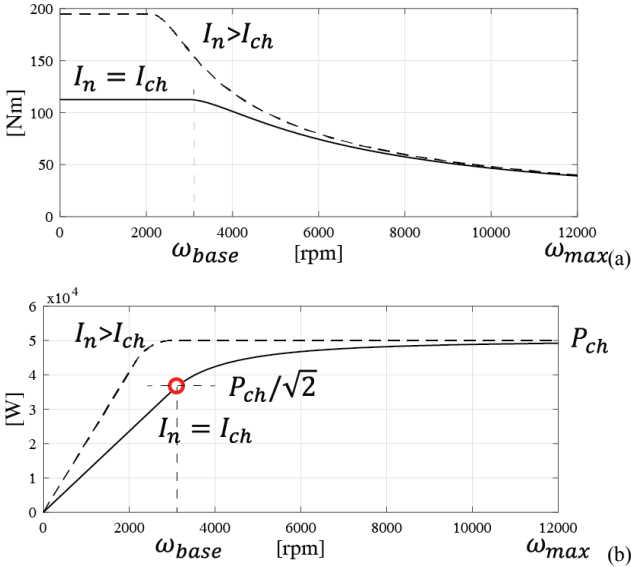

Fig. 2. Torque and power versus profiles under characteristic current and limited inverter voltage conditions. Two designs are reported: one with rated current equal to I_{ch} (continuous line) and rated current greater than I_{ch} (dashed line).
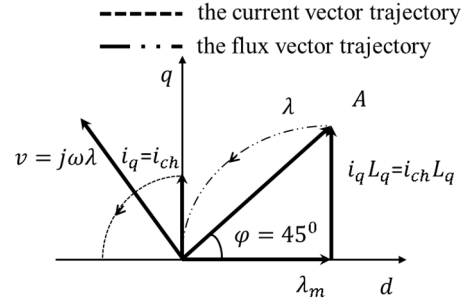

Fig. 3. Vector diagram of the CW-SPM machine with I_{ch} applied on the q axis

A. Nominal PF as the Metrics of the Flux Weakening Range

When the SPM machine is fed with its characteristic current, the vector diagram is the one in Fig. 3. Neglected the stator resistance voltage, when the current vector aligned to the q axis (point A), the (nominal) power factor is equal to $1/\sqrt{2}$ [11].

The flux weakening trajectories of the vectors are shown, with the current vector rotated counter-clockwise and the flux linkage trajectory eventually collapsing into the origin, producing the ideal power versus speed curve described above (Fig. 2). Therefore, the design condition $(PF)_n = 1/\sqrt{2}$ gives important insights on the flux weakening capability of one motor design. The design of a CW-SPM machine having a $PF = 1/\sqrt{2}$ at rated torque, condensates the twofold design specs (torque at low speed and power at high speed) into a single operating point, easy to define (current on the q axis). Roughly speaking, the torque target will define the machine size, given the cooling capacity, then the $PF = 1/\sqrt{2}$ condition will guide the tradeoff between PM flux linkage and armature inductance optimizing the flux weakening properties of the machine. In turn:

$$(PF)_n = \frac{1}{\sqrt{2}} \; \rightarrow \; I_{ch} = I_n \quad (4)$$

$$(PF)_n < \frac{1}{\sqrt{2}} \; \rightarrow \; I_{ch} < I_n \quad (5)$$

Designing the machine after condition (4) produces torque and power profiles like the ones in Fig. 2 (continuous). Designing after (5) produces the profiles represented with dashed lines.

B. Set of Inputs

The two design goals are torque at standstill and power at maximum speed, in nominal current conditions. With reference to the machine's ratings reported in Table 1, the parameters defined offline, prior to the design are:

- stack dimensions D, L [mm] and airgap length g [mm]
- Pole pairs p and winding type q (slots/pole/phase)
- PM remanence B_r [T] and peak flux density in steel B_{Fe} [T].
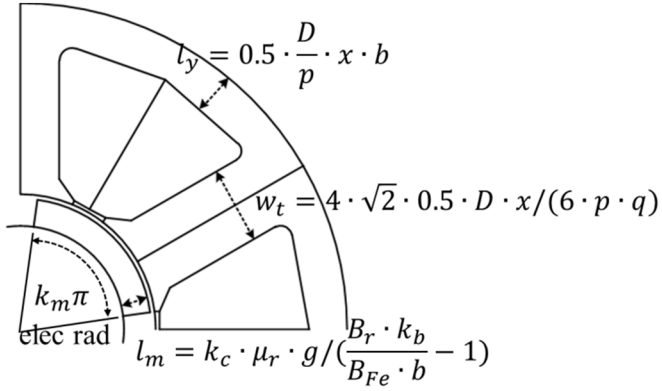- Electric loading, via the specific loss factor k_j [W/m^2].

$$l_y = 0.5 \cdot \frac{D}{p} \cdot x \cdot b$$

$$w_t = 4 \cdot \sqrt{2} \cdot 0.5 \cdot D \cdot x/(6 \cdot p \cdot q)$$

$$k_m \pi$$
elec rad
$$l_m = k_c \cdot \mu_r \cdot g / (\frac{B_r \cdot k_b}{B_{Fe} \cdot b} - 1)$$

Fig. 4. Definition of w_t, l_y and l_m as a function of design parameters x,b.

TABLE I RATINGS OF THE MACHINE

Machine type		CW-SPM
Pole pairs (p)		2
Stator slots (q)		6
Torque target	Nm	120
Maximum speed	rpm	12000
Power target, at max. speed	kW	45
Stator diameter (D)	mm	216
Length (L)	mm	170
Copper loss	W	1400
Specific loss factor (k_j)	kW/m^2	12.1
Airgap	mm	1.5
Copper filling factor		0.55
Steel grade		M250-35A
Steel loading (B_{Fe})	T (pk)	1.5
PM type		BMN-38EH
Remanence (B_r)	T	1.02 T @ 150°C
Converter voltage	V pk	173
Converter current	A pk	360
Rotor temperature	°C	150
Winding temperature	°C	130

The specific loss factor k_j [W/m^2] defines the level of electric loading indirectly. Considering only copper loss (stall conditions), such factor is:

$$k_j = \frac{Copper\ loss}{\pi DL} = \frac{(6N_s I)^2}{\frac{k_{Cu}}{\rho} \frac{L}{L+l_{end}} \cdot 2\pi D \cdot A_{slots}} \quad (6)$$

Where A_{slots} [m^2] is the total slot cross section (all slots), k_{Cu} is the slot filling factor (net copper on net slot), l_{end} [m] the end-turn length, ρ [Ωm] the resistivity of copper and N_s is the number of turns.

As said, the loss factor k_j (6) defines the electric loading A_s [A/m] of the machine:

$$A_s = \frac{6N_s I}{2\pi r} \propto \sqrt{k_j} \quad (7)$$

k_j is used in place of A_s because it contains information on stator and rotor quantities, whereas the electric loading refers to the rotor size only (r is the rotor radius). Moreover, k_j is more intimately related to the copper temperature. The value of k_j is selected from typical values for the type of cooling in use and verified with the help of a thermal network. A value of 12.1 [kW/m^2] was chosen here, considered typical of water cooling in automotive environment.

C. Design Plane x,b

The torque-PF design plane is defined after the two normalized design factors x and b:

$$x = \frac{r}{R} \quad (8)$$

$$b = B_{g1} / B_{Fe} \quad (9)$$

The former is easily defined as the rotor/stator split ratio, being r the rotor radius and R the stator outer radius. The latter factor b is the ratio of the airgap peak of the fundamental flux density B_{g1} and the iron peak flux density B_{Fe}.

The airgap flux density B_g (assumed to be constant under each pole) and the peak of the fundamental are related through the shape factor (k_b), defined as in [14]:

$$k_b = \frac{B_{g1}}{B_g} = \frac{4}{\pi} \cdot \sin(\frac{\pi}{2} \cdot k_m) \quad (10)$$

Where $k_m \pi$ is the magnet pole arc expressed in electrical radians, defined in Fig. 4. In this research, k_m is set to 5/6, for simplicity.

After B_{Fe} is set (for example 1.5 T stands for standard silicon steel sheets), the factor b defines B_{g1} and therefore the tooth and back iron widths w_t and l_y:

$$w_t = 4 \cdot \sqrt{2} \cdot 0.5 \cdot D \cdot x \cdot b/(6 \cdot p \cdot q) \quad (11)$$

$$l_y = 0.5 \cdot \frac{D}{p} \cdot x \cdot b \quad (12)$$

Where D is the stator outer diameter, p is the number of pole pairs and q is the number of slots per pole per phase. Given the airgap length and the PM remanence, the factor b also defines the PM length l_m [10],

$$l_m = k_c \cdot \mu_r \cdot g / (\frac{k_b \cdot B_r}{B_{Fe} \cdot b} - 1) \quad (13)$$

The symbols in (13) are Carter coefficient (k_c), airgap length (g), permeability (μ_r).

D. Torque and Power Factor Expressions

Torque and PF are expressed in terms of the two parameters x,b, using analytical expressions mutated mostly from [15]-[16], reviewed in the following. At low speed the current vector is controlled on the q axis, in quadrature with the PM flux linkage (λ_m, along the d axis). Therefore torque is:

$$T = \frac{3}{2} \cdot p \cdot \lambda_m \cdot i_q = \frac{3}{2} \cdot p \cdot \lambda_m \cdot I \qquad (14)$$

Where I is the current amplitude. The magnet flux λ_m expressed in terms of x and b is:

$$\lambda_d = \frac{\pi \cdot D/2 \cdot L \cdot N_s \cdot B_{Fe}}{\sqrt{3} \cdot p} \cdot x \cdot b \qquad (15)$$

The current amplitude is a function of the loading factor, the dimensions and the number of turns:

$$i_q = I = \frac{1}{6N_s} \sqrt{k_j \cdot \left(\frac{k_{Cu}}{\rho} \frac{L}{L+l_{end}} \cdot 2\pi D \cdot A_{slots} \right)} \qquad (16)$$

Where A_{slots} is dependent on both x and b: when x becomes larger, the stator area turns to smaller, which means A_{slots} is lower. The same is valid for b: a larger b means thicker teeth and yoke, so smaller slots. l_{end} in (16) is the length of the end turns, that is dependent on x,

$$l_{end} = 2l_t + 0.5(w_t + 0.5\pi(D \cdot x + l_t) \cdot sin(\frac{\pi}{6 \cdot p \cdot q})) \quad (17)$$

The PF is defined as:

$$PF = \cos(\varphi) \cong \frac{\lambda_d}{\sqrt{\lambda_d^2 + (L_q \cdot i_q)^2}} \qquad (18)$$

Where $L_q = L_d = L$ can be expressed in function of x, b using the mathematics. The inductance consists of magnetizing inductance L_m[15], slot leakage inductance L_{slot}, and tooth tip leakage inductance L_{tip}:

$$L_m = \frac{3}{2} \cdot \frac{8}{\pi} \cdot \left(\frac{k_w N_s}{p} \right)^2 \cdot \mu_0 \cdot l \cdot \frac{D \cdot x}{l_m + k_c \cdot g} \qquad (19)$$

$$L_{slot} = \frac{12}{6 \cdot p \cdot q} \cdot k_s \cdot \mu_0 \cdot l \cdot N_s^2 \qquad (20)$$

$$L_{tip} = \frac{12}{6 \cdot p \cdot q} \cdot k_t \cdot \mu_0 \cdot l \cdot N_s^2 \qquad (21)$$

Where k_w is the winding factor, k_s and k_t are permeance factors for slot leakage inductance and tooth tip leakage inductance respectively, dependent on slot sharp [17].
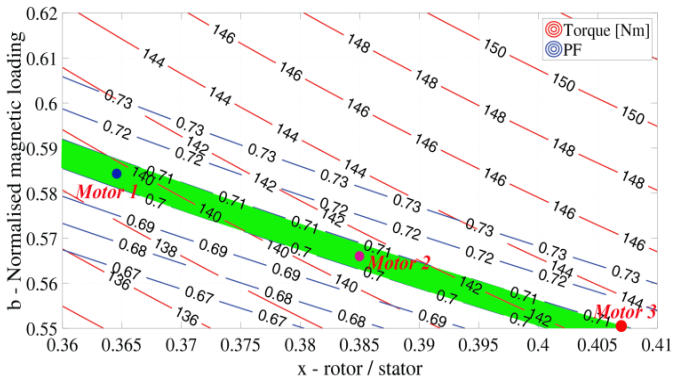

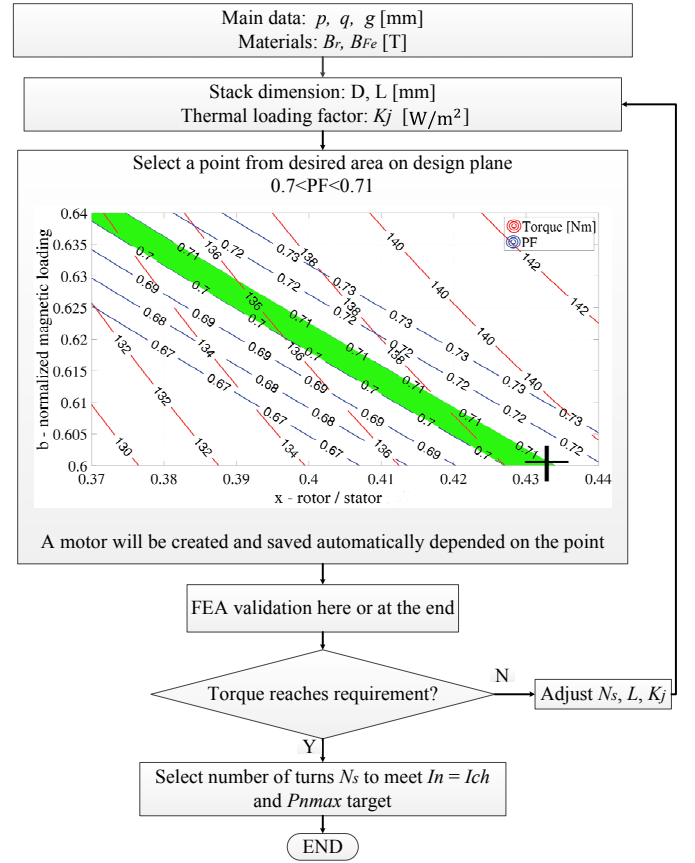Fig. 5.   T(x,b) and PF(x,b) design plane

Fig. 6.   Flowchart of the design procedure

Finally, the torque and PF contours are built in the x,b design plane, using the parametric expressions T(x,b) (14) and PF(x,b) (18). The chart is reported in Fig. 5. The subdomain of those solutions in the area with $PF = 1/\sqrt{2}$ is considered here, highlighted in green in Fig. 5. All machines in the green band have a flat power curve and infinite constant power speed range at nominal current. Among those, the ones with a higher torque in the chart will also produce higher output power at high speed. For example, motor 1 in Fig. 5 will give slightly less torque and power than motor 3.
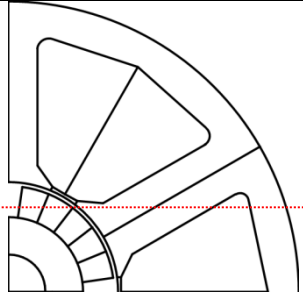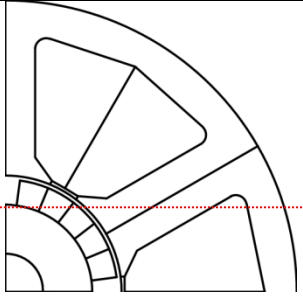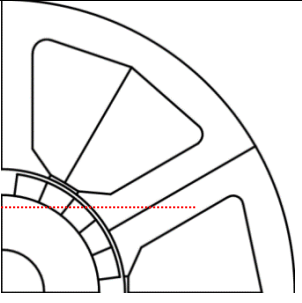
E. Design Flowchart

The airgap length is lower-limited by mechanical design considerations [15]. The number of pole pairs is set to two in order to limit the iron and PM losses at high speed. The choice of q= 0.5 is compatible with $p = 2$, because other effective fractional slot combinations (e.g. q= 2/5, 2/7) would require p>2 and thus higher rotational loss.

From the aggregate of the inputs, the T(x,b) - PF(x,b) design plane is built. The region $0.7 < PF < 0.71$ is the target design area, around the condition $PF = \sqrt{2}$. Within this region, the higher torque producing capability can be read from T(x,b).

Three feasible designs are selected and analyzed further (motors 1 to 3 indicated in Fig. 5). The adopted design software (Syr-e [12]) runs the x,b procedure and can build the FEA model of any motor seamlessly. A comparison between

TABLE II COMPARISON BETWEEN ESTIMATED AND FEA RESULTS

Motor Number	1		2		3	
(x, b)	(0.363, 0.585)		(0.385, 0.57)		(0.404,0.55)	
Structure						
l_m	11.54		9.41		8.01	
	Model	*FEA*	*Model*	*FEA*	*Model*	*FEA*
Torque [Nm]	139.6	129.5	141.2	131.1	143	131.3
PF	0.705	0.71	0.706	0.707	0.71	0.701

model and FEA is reported in Table 2, showing pretty good agreement. Saturation plays a role in these machines, but do not harm the accuracy of the model. The fulfillment of the torque target can be FEA verified at this moment or at the end. If the target torque is not met, either the stack size (*D, L*) or the loading (k_j) should be modified and the process iterated.

After the torque target is met, the tuning of the output power to the target comes very easily through the design of the number of turns N_s. As shown in (4), the loading input k_j determines the Ampere-turns product $N_s I$ altogether, but not the number of turns and neither the current alone. Therefore, N_s is adjusted so that the motor current equals the nominal value coming from (1) and (2).

$$I_n = P_{nmax} / \left(\frac{3}{2} V_{max} \right) \quad (22)$$

F. Demagnetization limit

Magnet thickness must be lower and upper limited to avoid the risk of demagnetization, on the one side, and excess of PM loss, on the other side. If PMs are too thin they tend to demagnetize early with load, whereas if they are too thick the eddy current loss increase without any torque or power output advantage.

The flux density of PM B_m is assumed to be equal to B_g. Therefore,

$$B_m \cong B_g = B_r / (k_b + k_b \cdot k_c \cdot \mu_r \cdot \frac{g}{l_m}) \quad (23)$$

From (9), (10) and (23), the ratio l_m/g determines the airgap flux density and the loading of the magnet. It is:

$$l_m/g = k_c \cdot \mu_r / (\frac{B_r}{B_{Fe} \cdot b} - 1) \quad (24)$$
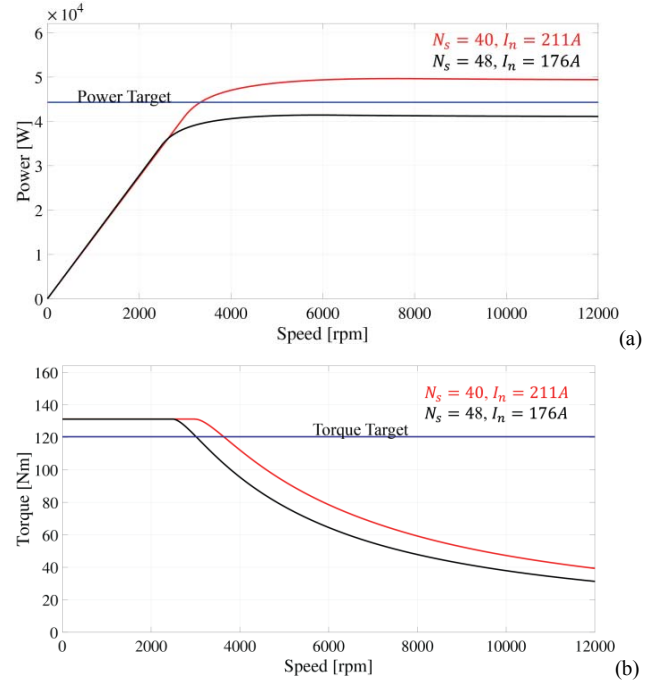

(a)

(b)

Fig. 7. Power (a) and torque (b) profiles of motor #3, for same k_j [W/m²] and different number of turns.

If l_m/g is limited between 3.5 and 6.5, this turns into a limitation of the range of *b*, according to (24). With $B_r = 1.02\,T$. This turns into

$$\frac{1.02}{\frac{k_c \cdot \mu_r \cdot B_{Fe}}{3.5} + B_{Fe}} < b < \frac{1.02}{\frac{k_c \cdot \mu_r \cdot B_{Fe}}{6.5} + B_{Fe}} \quad (25)$$

III. RESULTS

A. Design Examples

Three designs were chosen from the (x,b) plane of Fig. 5, they are shown in Table 2. Comparison between model and FEA results is reported in the table. Motor#3 was selected as the best candidate because: 1) it has the highest torque forecast. 2) It has the largest x value, therefore the biggest rotor, and the shortest teeth and, ultimately, less copper and shorter end connections. Moreover, it eases thermal exchange from copper to coolant. 3) The volume of magnet is the smallest among the three.

B. Power and Torque Envelopes

The FEA calculated power and torque envelopes of motor #3 are presented in Fig.7. It is shown how the number of turns N_s modifies the height of the power plateau and not nominal torque. The Ampere-turns product N_sI, coming from the design input k_j is the same, so torque is the same. As N_s decreases, the characteristic current, characteristic power, and base speed all grow (Fig. 7). The power requirement is met here when the number of turns decreases from 48 to 40 (45 kW).

Fig 8 reports the power profile of motor #3. Under the maximum current condition, the power generated at high speed is the same as power produced under characteristic current condition. Around the base speed, power produced under maximum current condition is a bit higher, which confirms that over-loading a CW-SPM motor over its characteristic current level is not an effective means of having more output power.

Although the over-load capability is nearly none, the losses from over-load condition are much higher than those from characteristic or below characteristic conditions (Fig. 9). The over-load losses may be more than double the losses from characteristic condition.

Fig.10 reports the FEA calculated efficiency map of the final design. Segmentations (5 x 5) are applied for PMs in both circumferential and axial directions to reduce the eddy current effects on PMs. The motor achieves high efficiency over a large proportion of the operating area. Nevertheless, burdened with heavy losses, the efficiency drops under over-load condition or in high speed operating region.
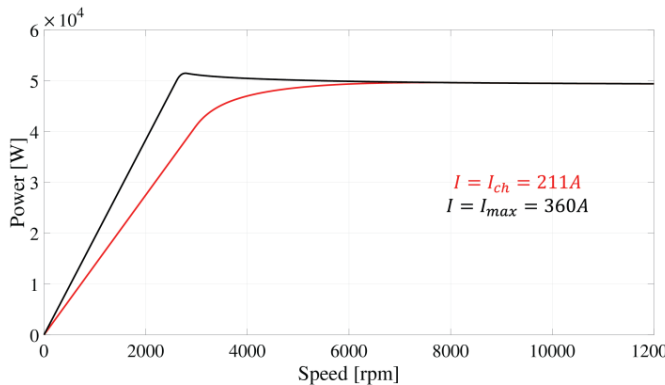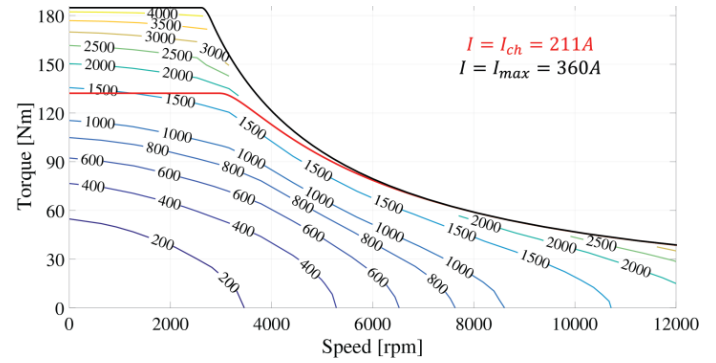

Fig. 8. Power profile for motor #3

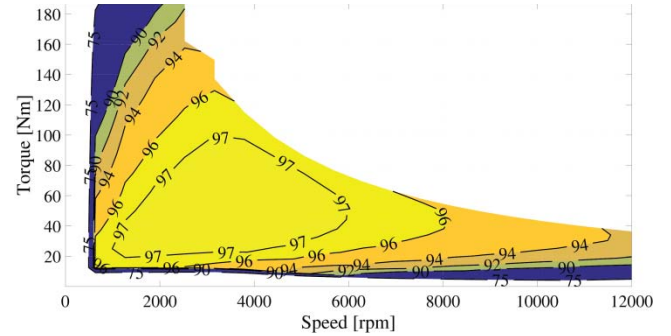Fig. 9. Loss map and torque profile of motor #3

Fig. 10. Efficiency map of motor #3

IV. CONCLUSION

A straightforward design approach was presented, for CW-SPM for traction applications. The x,b design plane was introduced, to match torque requirement and the key design condition of power factor equal to $1/\sqrt{2}$. All designed machines have infinite speed flux weakening range. The illustrated design method for CW-SPM simplifies the design process, compared with general design procedures. The model used for the parametric design was FEA validated with success. Design equations will be comprehensively provided in this research. FEA is also used to characterize the final design and to get to torque/power profiles, the loss map and the efficiency map, by means of open source resources.

REFERENCES

[1] T.A. Burress, et Al., "Evaluation of the 2010 Toyota Prius Hybrid Synergy Drive System," U.S. Department of Energy Vehicle Technology, March 2011

[2] R.H. Staunton, T.A. Buress, and L.D. Marlino, "Evaluation of 2005 Honda Accord Hybrid Electric Drive System," U.S. Department of Energy Vehicle Technology, Sept. 2006

[3] A. M. EL-Refaie and T. M. Jahns, "Optimal flux weakening in surface PM machines using concentrated windings," *IEEE Trans. Ind*. Appl.,vol. 41, no. 3, pp. 790–800, May/Jun. 2005.

[4] F. Magnussen and C. Sadarangani, "Winding factors and Joule losses of permanent magnet machines with concentrated windings," *Electric Machines and Drives Conference, 2003. IEMDC'03. IEEE International*, 2003, pp. 333-339 vol.1.

[5] A. M. EL-Refaie, "Fractional-slot concentrated-windings synchronous permanent magnet machines: Opportunities and challenges," *IEEE Trans. Ind. Electron.*, vol. 57, no. 1, pp. 107–121, Jan. 2010.

[6] A. M. El-Refaie, T. M. Jahns and D. W. Novotny, "Analysis of surface permanent magnet machines with fractional-slot concentrated

windings," in *IEEE Transactions on Energy Conversion*, vol. 21, no. 1, pp. 34-43, March 2006.

[7] N. Bianchi, S. Bolognani and P. Frare, "Design criteria for high-efficiency SPM synchronous motors," in *IEEE Transactions on Energy Conversion*, vol. 21, no. 2, pp. 396-404, June 2006.

[8] J. Wang, X. Yuan and K. Atallah, "Design Optimization of a Surface-Mounted Permanent-Magnet Motor With Concentrated Windings for Electric Vehicle Applications," in *IEEE Transactions on Vehicular Technology*, vol. 62, no. 3, pp. 1053-1064, March 2013.

[9] Biais, F., and Ph Langry. "Optimization of a permanent magnet traction motor for electric vehicle." Colloque sur les véhicules électriques et hybrides. 1999.

[10] B. Boazzo, G. Pellegrino, A. Vagati, "Multipolar SPM Machines for direct-drive application: a general design approach," *IEEE Trans. Ind. Appl.*, vol. 50, no. 1, pp. 327-338, Jan.-Feb. 2014.

[11] W. L. Soong and T. J. E. Miller, "Field-weakening performance of brushless synchronous AC motor drives," in *IEE Proceedings - Electric Power Applications*, vol. 141, no. 6, pp. 331-340, Nov 1994.

[12] Cupertino F. et al., "Syre - Synchronous Reluctance (machines) – evolution" [Online]. Available: http://sourceforge.net/projects/syr-e/ [Accessed: 10- Nov- 2015]

[13] D. Meeker. "Finite Element Method Magnetics (FEMM)". [Online]. Available: http://femm.foster-miller.net [Accessed: 10- Nov- 2015]

[14] K. F. Rasmussen, J. H. Davies, T. J. E. Miller, M. I. McGelp and M. Olaru, "Analytical and numerical computation of air-gap magnetic fields in brushless motors with surface permanent magnets," in *IEEE Transactions on Industry Applications*, vol. 36, no. 6, pp. 1547-1554, Nov/Dec 2000.

[15] Lipo, Thomas A. "Introduction to AC machine design", Wisconsin Power Electronics Research Center, University of Wisconsin, 2014.

[16] D. Hanselman , "Brushless Permanent Magnet Motor Design", University of Maine, 2003.

[17] Pyrhonen, Juha, Design of rotating electrical machines, 1st ed. John Wiley & Sons, 2008.